RESEARCH ARTICLE

A MATLAB-Based Toolbox to Simulate Transcranial Direct-Current Stimulation Using Flexible, Fast, and High Quality Tetrahedral Mesh Generation

AMJED Y. SAHIB[1], **HADI SEYEDARABI**[1], **REZA AFROUZIAN**[2], **AND MEHDI FARHOUDI**[3]
[1]Faculty of Electrical and Computer Engineering, University of Tabriz, Tabriz 51368, Iran
[2]Miyaneh Faculty of Engineering, University of Tabriz, Miyaneh 51368, Iran
[3]Neurosciences Research Center (NSRC), Tabriz University of Medical Sciences, Tabriz 51368, Iran

Corresponding author: Reza Afrouzian (afrouzian@tabrizu.ac.ir)

ABSTRACT In numerical computation of neuromodulator such as transcranial direct current stimulation (tDCS) and transcranial magnetic stimulation (TMS), the quality of the tetrahedral mesh is a significant criterion to achieve accurate results in simulating the electric field distribution. Although there are various algorithms and software products have been proposed to achieve this goal, but most of them have challenges in ease of use or in the quality of the final mesh. Even with the production of tetrahedral mesh, there is still a deficiency in the quality of the tetrahedral mesh that leads to reduced accuracy in the final result. In this paper, a new MATLAB toolbox (SimUTab) is presented that uses several useful algorithms in this field and also employs new methods to generate high-quality meshes for head models. The proposed method reduces the difficulties and makes it easy to use. The user interface implemented in MATLAB makes easily designing electrodes even with unusual shapes and hence provides the basis for examining the effect of electrode shapes on the electric field distribution of the target area. The proposed method is tested and compared with other active pipelines. The results confirm the superiority of the proposed method and show an improvement in the quality of the final mesh.

INDEX TERMS Transcranial direct current stimulation, structural magnetic resonance segmentation, finite elements method (FEM) analysis, forward electric field calculation.

I. INTRODUCTION

In the past three decades, tDCS has come to be attention from many researchers. tDCS is a non-invasive technique used to stimulate a specific area of the brain by applying a weak current, which induces a specific shift in the excitability of the target brain cells [1]. Determining how the electric field is distributed in the human brain through this method is challenging. Cortical folding is complicated that causes an inhomogeneous connection of the applied current in the brain. In the tDCS technique, no imaging method has yet been able to record the electric field distribution of the applied DC current. As consequence, the estimation of the

The associate editor coordinating the review of this manuscript and approving it for publication was G. R. Sinha.

electric field distribution in the brain is investigated through computer-based numerical simulation.

In tDCS method, the stimulation process is performed by placing pair or multi-electrodes in previously defined positions on the scalp to stimulate the targeted brain area with small amounts of current (1-2 mA) [2]. Typically, increasing the electric field concentration in the target area of the patient's brain improves the modulation of neural pathways in that area and helps in the rapid treatment of brain injuries [3]. On the other hand, the current injected by the electrodes passes through different layers as well as their interfaces with variant electrical properties to reach the target area. Hence, it is difficult to accurately predict the required current (at the electrodes) to achieve the desired current density in the target area. In particular, some obstacles limit the current

of electrodes such as low connectivity of the scalp (resulting in a shutting effect where the electric field is spread) [4]–[6]. In addition, due to safety considerations, the amount of injected current should be precisely adjusted to prevent undesired consequences such as skin burns, itching, fatigue, headache and phosphine [3], [7]. Thus, some researchers have particularly focused on improving the focality of electric field in the target area. For this purpose, they have tried to extend the electric field to the depths of the brain by optimizing the position of electrodes or designing new shapes. The above solution can be better than increasing the current injected by electrodes, which has the mentioned adverse effects [8], [9]. Golestanirad *et al.* [10] showed that employing the modified fractal topology in designing the electrode shapes can increase nerve stimulation and also density of electric field. In other words, by maintaining the same activation levels of neurons, it reduces the required delivered power by 22%. After that, Mahdavi *et al.* [11] continued the work of Golestanirad through modeling by FEM to investigate the effect of geometric changes on the current density distribution and compared it with the conventional electrodes. The results shows that the current density produced by the newly formed electrodes is 1.3 times higher than conventional electrodes. Recently, in a work by Amani *et al.*, new shapes of electrodes have been modeled to investigate their impact on the rehabilitation of patients suffering from post-stroke Aphasia [12]. The authors illustrate that when electrodes with edginess surfaces are used, the electric filed distribution is significantly increase in the target area.

In previous methods, simplified spherical models have been used to estimate distribution; so that they have captured general features of spatial field distribution [5], [13]. Some reports indicate a significant deviation between the simplified model and the use of a realistic head model based on individual MRI of the patient [14]–[16]. However, simulation-based on a realistic head model involves many steps with methodological difficulties. This type of simulation limits the variety in the algorithm stages and increases the complexity in the software implementation. On the other hand, due to the need to manually correct the defects accrued after each step, it requires much more execution time [17]. As a result, most studies are performed on a specific group of head models and their expansion into different types of head models is challenging. Hence, existing pipelines either lack such tools or need extensive interaction with other tools to achieve this goal. However, the demand to estimate electric field distribution on the realistic head model (MRI-based) has been increased to more accurately evaluate the neural activities [18]–[20]. For this purpose, many pipelines have been proposed which integrate software products with different methodologies to automate the process of head model reconstruction [21]–[24].

On the other hand, each pipeline has its own features that can be evaluated in terms of ease of use, anatomical display accuracy, the quality of the final mesh, flexibility in designing

electrodes, and their placement. However, two recent cases have more significance. In the first case, there is a growing demand on a tool that allows you to investigate the effectiveness of the electrodes with shapes other than conventional types (pad, circle) that increase the concentration of electric field in a specific area of the brain [8]. The next is the need to produce high-quality flexible mesh which provides two important advantages. The first is to increase the accuracy of the distribution field and the second is the high flexibility in using finite element software packages.

In this paper, the limitations are addressed and a new pipeline in the MATLAB environment is developed which has been named SimUTab. SimUTab is optimized in terms of ease to use, flexibility, computational cost, and execution time. A new capability has been added to SimUTab so that the user can (using an interactive graphical user interface (GUI)) easily design any shape of electrodes and place it anywhere on the head. Therefore, the user can quickly follow the effect of changes in the electrode shapes (as well as their position) on the electric field density in the target area. On the other hand, this article provides a new multi-step method to produce high quality tetrahedral mesh. To achieve this, some popular available software is utilized in various sections. Hence, the proposed toolbox tries to employ their capabilities together and design a new method (using them) to produce high-quality tetrahedral mesh. Of course, in during putting them sequentially, there are some challenges. Therefore, to manage them, this article considers some innovations in various parts of the proposed method.

The rest of the article is organized as follows: the proposed method is explained in detail in section 2. FEM evaluation is demonstrated in section 3. In section 4, results and discussion are reported and in the last section, conclusions are described.

II. METHODS
A. TOOLBOX OVERVIEW
To simulate the electric field distribution in the MRI-based model, several steps are considered in the form of a pipeline, which can be seen in Fig. 1. In the proposed workflow, several software products are utilized and integrated to build an optimal simulation system. The proposed workflow is implemented in a MATLAB environment and two popular toolboxes, statistical parametric mapping (SPM12) [25] and Neuroimaging Informatics Technology Initiative (NIFTI) [26] are employed. It has an easy-to-use GUI which allows users to perform all the simulation steps interactively without having to write any code. In the proposed pipeline, several parameters can be changed interactively, such as regularization parameter in the image segmentation step, surface mesh density, tetrahedral mesh density and threshold quality which will be explained in the next sections. As well, an interactive interface is considered that allows users to easily draw any shape of the electrode. Fig. 1 shows the steps performed in the pipeline to simulate the distribution of an electric field.
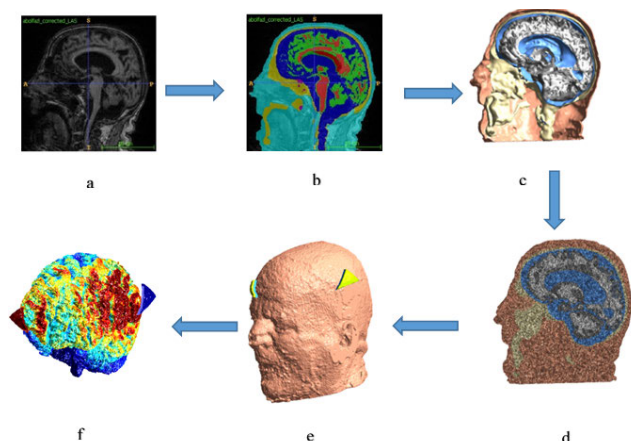
FIGURE 1. Overview of the proposed pipeline to simulate the electric field in the real head model (a) preparation of MRI image (b) segmentation (c) surface mesh generation of each tissue and overlaying (d) error correction and volume mesh generation (e) generation of electrodes meshes and projection on the head mesh (f) finally, solving the FEM model.

In the pipeline, at first, to adjust the orientation of MRI in the segmentation step, the NIFTI toolbox is employed. Then, in the next step, the SPM12 toolbox is used to segment the head. In the third section, cleaning of segmented tissue is performed. After that, in the fourth step, a triangular surface in each tissue mask is created and optimized. Then, (fifth step), the volumetric mesh of the entire head is created. The sixth stage involves putting and modeling the electrodes on the head. Finally, the last step simulates the electric field on the realistic head model based on individual MRI of the patient. The flowchart of SimUTab is shown in Fig. 2, each section of which will be explained in detail in the following sections of the article.

B. INPUT DATA

The type of input data employed in this toolbox is Structural magnetic resonance images (MRI). To enhance the structural details, two weighted-T1 images are considered for each participant, one with fat-suppression and the other without, as shown respectively in Table 1. The purpose of employing fat-suppression imaging is to attenuate the signal belonging to the spongy bone of the cranium and to intensify the signal belonging to other soft anatomical tissues such as Cerebrospinal fluid (CSF), gray matter (GM) and white matter (WM). This improves the accuracy of the boundaries in the tissue layers. Moreover, for better segmentation and to improve the separation border between the cranium and cerebrospinal fluid (CSF), T2-weighted images are employed as shown in Table 1. In order to validate and compare the proposed method with similar works, the standard average MRI of heads (New York Head) has been used [27].

C. SEGMENTATION AND CORRECTION

In the first step, segmentation and error correction is performed. To achieve this, a probabilistic framework presented
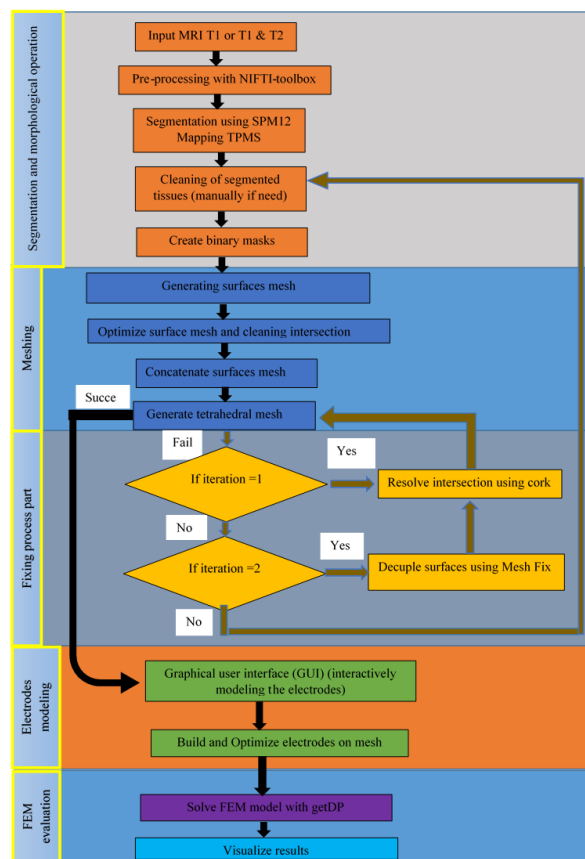

FIGURE 2. Flowchart of the proposed toolbox (SimUTab).

TABLE 1. Properties of input data include T1-weighted and T2-weighted images.

Images	Matrix size	Voxel size	Sagittal slice	flip angle	Reputation time (TR)	Time to echo (TE)	Inversion time (TI)
T1-weighted without fat suppression	183*280	1mm^3	160	20°	$4,650_{ms}$	$2,45_{ms}$	$1,200_{ms}$
T1-weighted with fat suppression	183*280	1mm^3	160	20°	$4,650_{ms}$	$4,220_{ms}$	$1,200_{ms}$
T2-weighted without fat suppression	201*230	1*1*2	90	105°	$11,500_{ms}$	102_{ms}	–
T2-weighted with fat suppression	201*230	1*1*2	92	110°	$11,800_{ms}$	310_{ms}	–

by Ashburner and Friston is used which is implemented in MATLAB (SPM12) [28]. For segmentation of tissue layers, SPM12 matches the histogram of the probability intensity (for input tissues) to the probability intensity histogram of prior tissues (Template) to determine the class of each voxel. The default Template used in SPM12 does not involve the
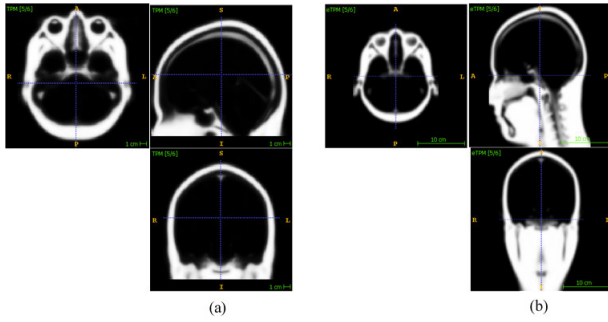
FIGURE 3. Templates used for MRI-head segmentation (a) default SPM Template (b) the template presented in [17] which includes the neck region.

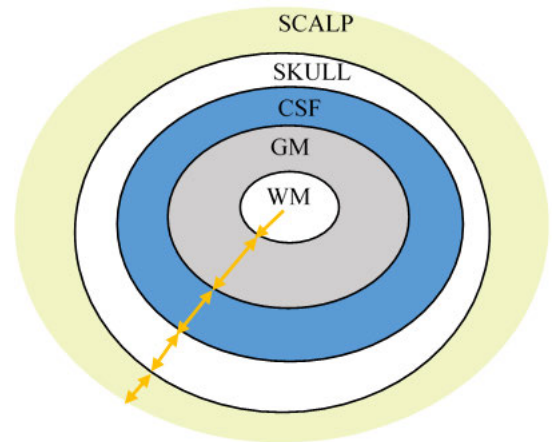**FIGURE 4.** Topological approach, which is followed in the proposed toolbox.

lower part of the head (neck) which is an essential region in the tDCS simulation process. Hence, for the neck, the template presented by Huang is used as shown in Fig. 3 [17]. The SPM12 generates probability maps to determine the most likely texture for each voxel. Therefore, the binary mask for each tissue is created. However, some defects still exist in the binary masks that require simple morphological operations to eliminate. The algorithm introduced by Huang *et al.* is employed to eliminate the defects. As mentioned above, the SPM12 generates six tissue layers, which are assumed to be enclosed by each other incrementally, so that WM and the scalp are innermost, and outermost layers respectively. Such a hypothesis is considered in previous works [17], [29], [30]. Sometimes, inaccurate segmentation may occur due to noisy MRI images. Hence, the above hypothesis may not be valid in regions where two tissue layers share the same boundary or the inner layer extends beyond the outer layer. This phenomenon leads to an intersection in the subsequent layer. Therefore, the need for more morphological operation is necessary. The proposed toolbox employs a method that truncates the inner layer, which extends beyond the outer layer. In addition, to prevent share boundaries, a small gap is inserted between two adjacent tissue layers to enforce the mentioned assumption as shown in Fig. 4. As proposed in [24] the above assumption can be achieved by modifying the outer layer of two adjacent layers through equation 1:

$$L_{outer} = max\left\{L_{outer} + L_{inner}, D_\xi(L_{inner})\right\} \quad (1)$$

where, (L_{outer}) and (L_{inner}) represent the outer and the inner layer respectively. Here D_ξ represents a max-filter which can be defined as a dilation operation in which replacing voxel with maximum value in the cubic neighboring region with half-edge distance (ξ) and can be defined as follows:

$$D_\xi(mask) : mask(i, j, k) =$$
$$max\left\{mask(i\pm \triangle i, j\pm \triangle j, k\pm \triangle k)_{-\xi \leq \triangle \leq +\xi}\right\} \quad (2)$$

the value of ξ is set to one to minimize distortion of the main tissue layer [24]. It is important to mention that the above operators are only applied in the area where two adjacent layers almost intersect or their boundaries merge. All the

above morphological operations are employed to reduce the complexity of interlaced tissue layers in the human head model. Fig. 5(a) shows an example of segmentation error between WM and GM, which are marked with white circles, after applying the mentioned method, as shown in Fig. 5(b), the extended parts of WM are truncated. This process effectively reduces the mutual intersection that may occur between adjacent layers in the surface mesh creation step.
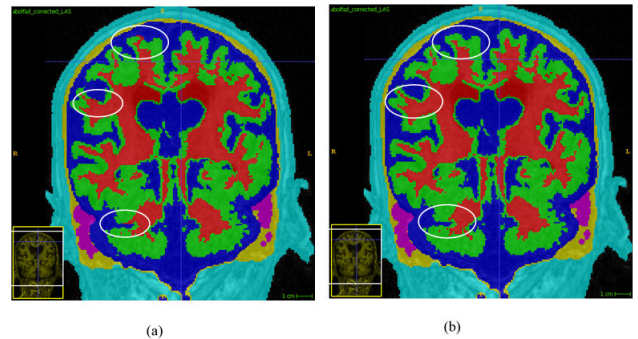
FIGURE 5. Zoomed coronal view of head MRI example with tissues mask overlaid on it (a) shows some extended parts from WM mask beyond GM mask or near mutual with GM (b) show overlaid masks after applying the correction routine.

### D. SURFACE MODEL GENERATION AND OPTIMIZATION
In the fourth step, to produce a high-quality mesh, surface meshes are extracted using probability masks which produced by the segmentation step. If surface meshes are not prepared carefully in this step, the subsequent procedure completely fails. In this step, surface extraction in each tissue layer is performed by the "ε-sample" algorithm [31] which is implemented in the Surface Mesh Generation Library(CGAL) [32]. CGAL allows us to define density and quality criteria for each layer. One of the most important parameters for CGAL is the iso-value, which in the present study is set to 0.3. If the iso-value is not fine-tuned, it will lead to incorrect results or the production of high-density surfaces. Fig. 6 shows the

mesh surfaces produced by different iso-values. However, there are still defects in the extracted triangular surface that lead to failure in tetrahedral generation step, such as self-intersection, isolated vertices (vertices that do not belong to any triangle surface), duplicated triangles and non-manifold vertices [33], [34]. To solve the mentioned deficiencies, two external tools are utilized, including Jmesh Library [34] and MeshFix [35]. Jmesh Library is used to remove non-manifold vertices, duplicated triangles and ensure the consistency of the triangles vertices order such that their normal is pointing outward. After cleaning, the tissue surfaces are concatenated to create the final head model. As previously explained, it is assumed that the layers are enclosed by each other incrementally. For example, WM is embedded in GM and GM in CSF and so on. Although morphological operation in the previous section dramatically reduces the chance of mutual intersection when surfaces are companies, some intersections may occur between adjacent tissue surfaces. A modified strategy based on Cork [36] and MeshFix is implemented to solve this problem. The process is done on the pairs from the inner tissue to the outer layer. When the surface of the tissue layer is extracted, then it needs to be combined with other tissue surfaces. Cork is used to resolve any intersection between concatenated surfaces. Consequently, the resolving process may lead to generating enclosed small regions between overlaid surfaces. These artifacts can be pre-processed and removed in the subsequent step. A strategy implemented in this pipeline is step-wise and time considering. So that when generating of tetrahedral mesh fails due to an error in the created surface mesh, it automatically tries to resolve the artifact iteratively. This process is automatically applied and repeated to eliminate various defects such as self-intersection, degenerate triangle, nearly degenerate triangle, and the mutual intersection. Finally, the output reaches the desired quality and the proposed pipeline then terminates the process loop. If still there is a mutual intersection and it leads to failure in the subsequent tetrahedral creation stage, the interface is added to manually repair the deficiencies and continue the repair process. The triangular surfaces are layer-specific where the Delaunay max radius is varying according to layer spatial distribution. In layers such as white matter and gray matter where these layers contain fine details, and should not be lost during surface extraction, the maximum Delaunay radius is chosen between 2-3 mm. In the region between pair of layers where they are mostly overlapped, the size of the mesh is chosen larger to another region. This wise mesh sizing is to prevent intersection between adjacent layers.

E. VOLUME MESH GENERATION

The mesh surfaces are produced and overlaid in the previous step. To fill these surfaces with high-quality tetrahedrons, an open-source Shewchuk's Delaunay refinement algorithm (TETGEN) is employed [37]. In some cases, small regions may be made up due to the surface mesh repairing process. These artifacts will be removed by calling TETGEN, Where TETGEN counts the overlaid surfaces in the
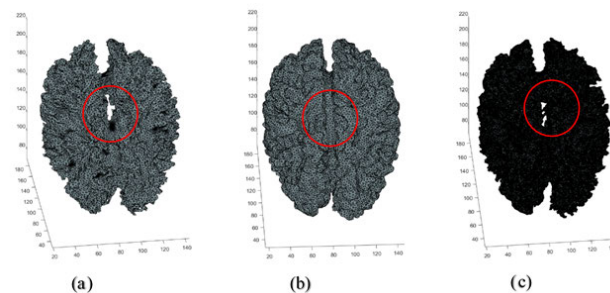
FIGURE 6. Surface mesh generation using different iso-values (a) with iso-value higher than 0.3 (b) with iso-value equal 0.3 (c) with iso-value less than 0.3 (very dense and inaccurate).

mesh and computes the internal point of each enclosed surface. Then it merges these small regions with the tissue surface to which they belong. Moreover, many options available in TETGEN allow the user to specify the quality and density of mesh generally or even for specific tissue layers. In the last part of volume meshing, an algorithm is added as a MATLAB script to preserve tissue surfaces boundary (preserving tissue actual shape)while at the same time keeping the mesh quality as high as possible. This can be achieved by utilizing the TETGEN meshing algorithm options, by forcing it to add strainer points in the internal domain of Piecewise Linear Complex (PLC) and prevent it from adding strainer points or modifying the boundary [39]. Also, TETGEN can enhance the overall quality of the mesh by specifying edge-ratio which will be explained in the next section.

F. MESH QUALITY MEASUREMENT

Low-quality output mesh affects both the convergence and method stability [40]. Therefore, generating mesh with high quality is crucial. There are a variety of metrics to measure the quality of the generated mesh. For example, as reported in [41] dihedral angle is used to measure the quality of mesh elements. another study, presented in [42] chooses the Edge-ratio of a tetrahedron as a quality metric where the ratio of the longest edge to its shortest edge is calculated to assess the mesh element's quality. In this article, the shape quality measurements from previous literature (that are widely used to analyze output mesh) are employed to judge the quality of resulted mesh [43]. After applying these measurements, the quality of mesh elements can be evaluated by estimation of the worst element shape and also obtaining the distribution of elements in terms of their quality. The first metric that assesses the quality of the tetrahedron mesh is Joe-Liu(η) [44] which is defined in equation 3 as:

$$\eta = \frac{12 * (3V)^{\frac{3}{2}}}{\sum_i l_i} \tag{3}$$

where, l_i is the edge length between vertices of a single tetrahedron as shown in Fig. 7 and V denoted the volume of

a single tetrahedron which can be defined as follows:

$$V = \frac{1}{6} \left[det \begin{bmatrix} 1 & x_1 & y_1 & z_1 \\ 1 & x_2 & y_2 & z_2 \\ 1 & x_3 & y_3 & z_3 \\ 1 & x_4 & y_4 & z_4 \end{bmatrix} \right] \qquad (4)$$
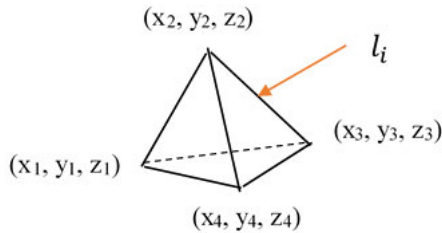

FIGURE 7. Single tetrahedron.

The second parameter used to measure the tetrahedron quality is the normalized edge-radius(α) [45] which be defined in equation 5:

$$\alpha = 2\sqrt{6} \left(\frac{r_{in}}{l_{max}} \right) \qquad (5)$$

where r_{in} is the radius of the inscribed sphere and l_{max} is the longest edge length of a single tetrahedron. The third metric criterion is the radius ration ρ [44] which can be defined as the ratio between the inradius to the circumradius of single tetrahedron, as given in equation 6:

$$\rho = 3 * \frac{r_{in}}{r_c} \qquad (6)$$

The range of all the above measurements metric is between 0 and 1. So that the lowest value indicates the quality score in the worst shape and the highest score indicates the quality value in the desired tetrahedron. In addition, the volume (V) of the tetrahedron can be assumed as another quality criterion. It is important to note that this volume for any particular tetrahedron needs to be more than the threshold value, which is equal to 10^{-4} (mm^3) [46]. In the tetrahedrons generating step, the volume of each particular tetrahedron is enforced by TETGEN to be more than the threshold value. Also, TETGEN enhances quality by using the edge-ratio criterion as the refinement termination condition [37]. It can be defined in equation 7:

$$Q = \frac{r_{out}}{l_{min}} \qquad (7)$$

where, r_{out} is the radius of the tetrahedron's circumscribed sphere and $l_{min}$is the shortest edge length of a single tetrahedron. The theoretical threshold bound of this ratio is equal to 0.612 at an equilateral tetrahedron [37]. The small Q indicates a high-quality tetrahedron contrariwise to other quality metrics.
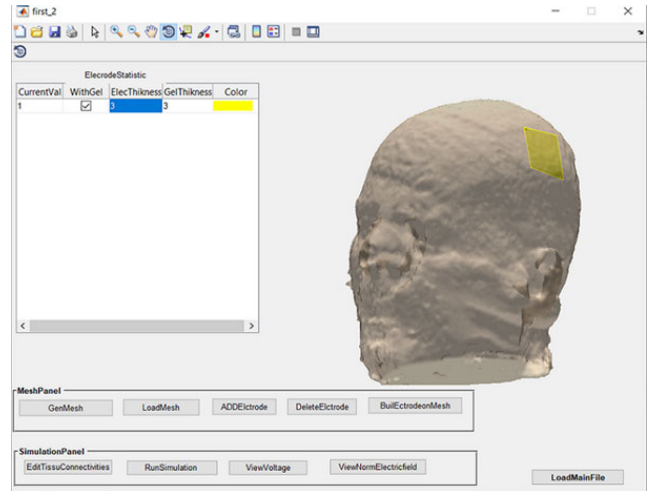

FIGURE 8. Graphical user interface (GUI) in main window of toolbox.

G. ELECTRODE PLACEMENT

In this step, designing and placing of the electrodes will be explained. As we can see in Fig. 8 the main window of designed GUI. This interface provides several tools that facilitate the placement of the electrodes even for inexpert users. It allows the user to assign the thickness (mm), the amount of injected current, and the use (or non-use) of the gel for each electrode. Another tool is shown in Fig. 9 which allows the user to plot electrodes with any shape. This makes the researchers examine a new shape easily without any need to write code.
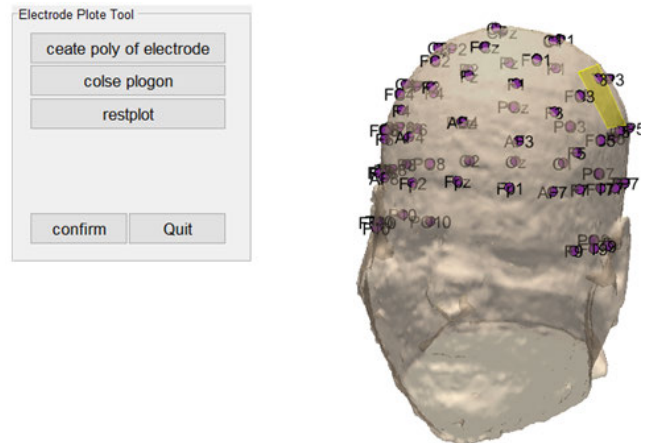

FIGURE 9. Assistant tool for drawing electrodes in any desired shape guided by (10-20) international system.

The challenges of electrode projection on the head are presented in [38] where the final mesh contains some intersections which cause the FEM solver to fail or reduce the output accuracy. This is shown in Fig. 10(a) Where intersections are marked with red points on the mesh. In this work, a smart procedure is followed by incorporating TETGEN and MeshFix to ensure there is no intersection between head surface mesh and electrode surface mesh. Fig. 10(b) shows the result of

repairing intersections and correcting surface triangles. This approach is implemented as a MATLAB script to create the electrode surfaces and project them on the head model and. then, the algorithm creates the volume mesh of electrodes that are projected on the scalp by employing TETGEN. A brief flow chart of the algorithm is shown in Fig. 11.
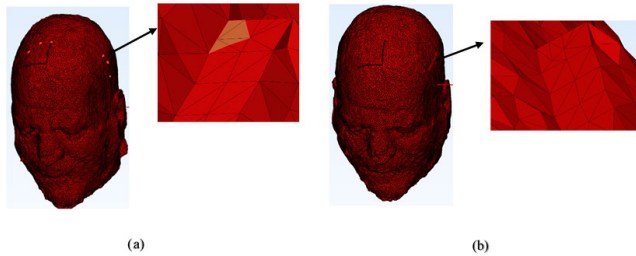
FIGURE 10. (a) Resulted mesh before repairing and contain some intersections and (b) after applying the proposed repairing method and all intersections are repaired.
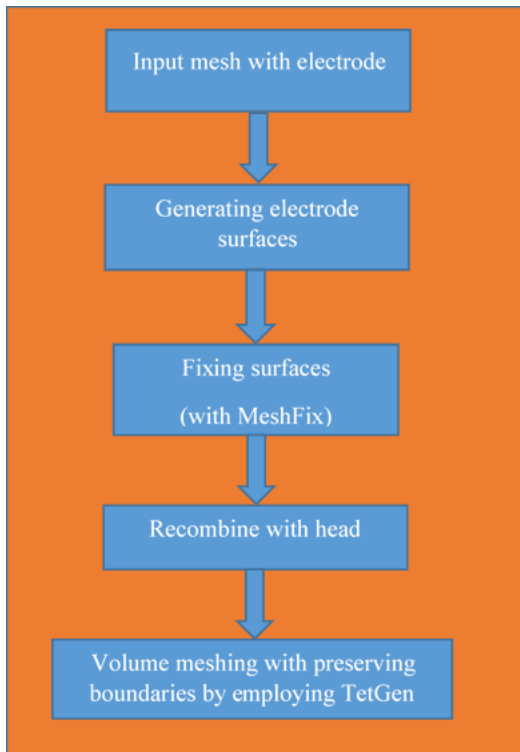
FIGURE 11. Brief flowchart of the algorithm for repairing and volume meshing of electrodes.

III. FEM EVALUATION

A. TISSUES CONNECTIVITY

The electrical conductivity of the human head cannot be accurately estimated with any imaging systems. The estimated connectivity values for each tissue layer are shown in Table 2 [47]. It is important to mention that there is an option in the proposed toolbox to edit the value of tissue connectivity as needed.

TABLE 2. Conductivity of various tissues in the human head.

No.	Tissue Type	Conductivity (σ)
1	WM	0.126
2	GM	0.276
3	CSF	1.654
4	Skull	0.01

B. BOUNDARY CONDITION

Before solving any finite element system, boundary conditions need to be set. In the proposed work, a Neumann boundary condition is considered at the outer boundaries and the amount of injected current is specified by the user for anode and cathode respectively. The outside air surrounding the skin acts as an insulator and the outer electrical potential of the skin has Neumann boundary condition with a zero gradient.

C. SOLVING FINITE ELEMENTS SYSTEM

The final head model mesh is categorized under the electrostatic problem. To solve such a problem, Maxwell's equations are employed. The employing of these equations provides a sufficiently approximate solution of the electrical field intensity and the density distribution of electrical current in the human head. The relationship between electrical potential field applied by electrodes and connectivity of tissues is formulated by a quasistatic form of Maxwell's equations [48] as described in equation 8:

$$\nabla(\sigma \nabla \phi) = 0 \tag{8}$$

where σ and ϕ are the connectivity of conductor tissue and applied electrical potential respectively. The electrical field intensity (E) can be found by partial derivative of electrical potential as given by equation 9:

$$E = -\nabla \phi \tag{9}$$

The electrical current density (J) can be computed from the linear relation given by equation 10:

$$J = \sigma E \tag{10}$$

The free open-source finite elements solver, getDP, is employed for estimating electrical field intensity [49]. This solver calculates the electrical field intensity and current density using the finite element method.

D. RESULTS VISUALIZATION

This section evaluates the proposed algorithm (SimUTab) in various aspects and compares it with other works in this field. As mentioned previously, SimUTab is implemented in the MATLAB environment. Also, OpenGL [50] is employed for increasing the graphics quality and reducing processing time.

IV. RESULTS

A. QUALITY OF GENERATED MESH

The output mesh from the mentioned steps contains six tissue layers WM, GM, CSF, SKULL, SKIN, air cavity,
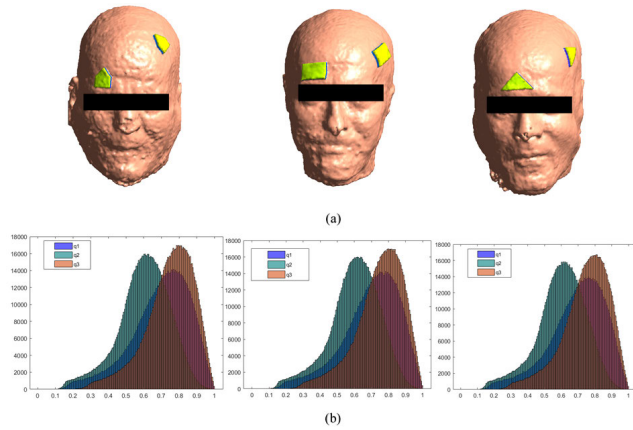
FIGURE 12. (a) Experiments using several head models with different electrodes assemblies. (b) Histograms of quality metrics for the above head models where q1, q2 and q3 represent Joe-Liu (η), normalized edge-radius ratio (α) and circumscribed to inscribed sphere radius ratio (σ) respectively.

TABLE 3. Mesh and quality metrics for three different experiments.

| Sub.	Tetra.-num.	Node num.	Value mean (ρ)	Value mean (α)	Value mean (η)
Expriment1	1086298	188532	0.722	0.613	0.7452
Expriment2	1092830	187673	0.695	0.6011	0.7464
Expriment3	1067805	185522	0.6994	0.5992	0.7447

and includes the electrodes mesh. Fig. 12(a) shows experiments using three head models with different electrodes assemblies performed using the proposed toolbox in this article. The overall surfaces are smooth and have high quality. In Fig. 12(b), histograms of quality metrics for each experiment confirm that the output mesh has high quality. The overall average quality measured for output meshes (created from our dataset) based on different quality criteria is Joe-Liu (η)=0.75±0.01, inscribed circumscribed radius sphere ratio (ρ)=0.7±0.02 and radius-edge ratio (α)=0.6±0.045. The output mesh has a relatively small number of nodes (with high-quality tetrahedral) which significantly reduces the cost of computation time. In addition, histogram of element volume is measured for these experiments as shown in Fig. 13. The measured volumes are all above the threshold, has no negative values (invalid or degenerate tetrahedrons) and well distributed [51]. The results of these experiments are summarized in Table 3. As mentioned above, one of the innovations in this article is to provide a way to resolve intersection which may occur in the projection of electrodes on the head. In order to evaluate the effectiveness of the mentioned method, as shown in Fig. 14, a standard head model from New York head is considered and electrodes placed on it using the proposed toolbox (Fig. 14(a)). Fig. 14(b) and (c) show the skewness histogram (one of
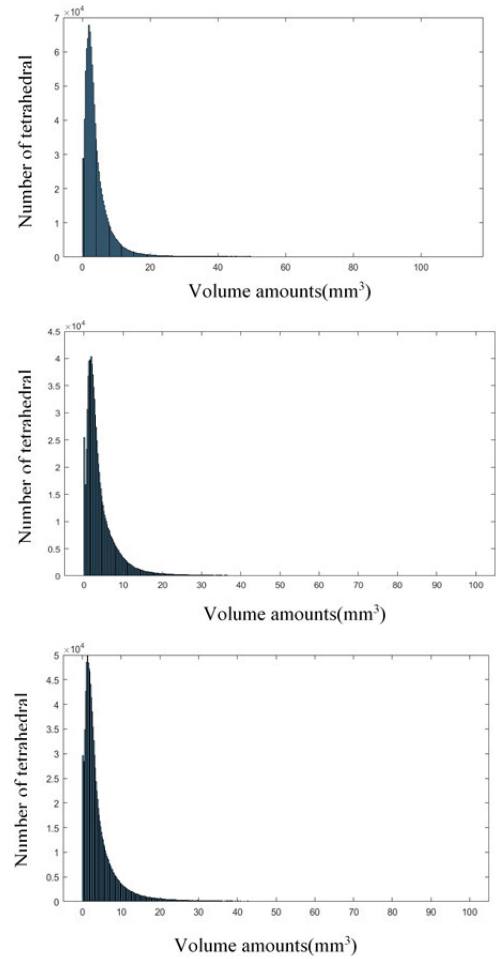
FIGURE 13. Histogram of elements volume for three described different head models shows that all elements has positive volume and there is no degenerate or invalid tetrahedrons.

the mesh evaluation criteria in COMSOL software [52]) before and after applying the correcting algorithm which has proposed in the SimUTab toolbox, respectively. According to COMSOL documentation [52] the output mesh (before correcting algorithm) contains degenerate and poorly tetrahedrons (minus values indicate degenerate tetrahedrons) which their quality has improved to the acceptance range for the FEM solver. Finally, Table 3 shows the mesh metrics (nodes and tetrahedrons) for various experiments (performed by SimUTab). As compared with previous works [53]–[55], despite the improvement in the quality of meshes; the number of nodes and tetrahedrons are dramatically reduced without the need for any more refinement. The mesh with the above specifications makes the FEM solver work accurately and reduces processing time in the subsequent steps. When the output mesh passes the agreed threshold for different FEM solvers (even complex ones such as COMSOL, Abaqus), there is flexibility in using different FEM programs for the generated mesh.
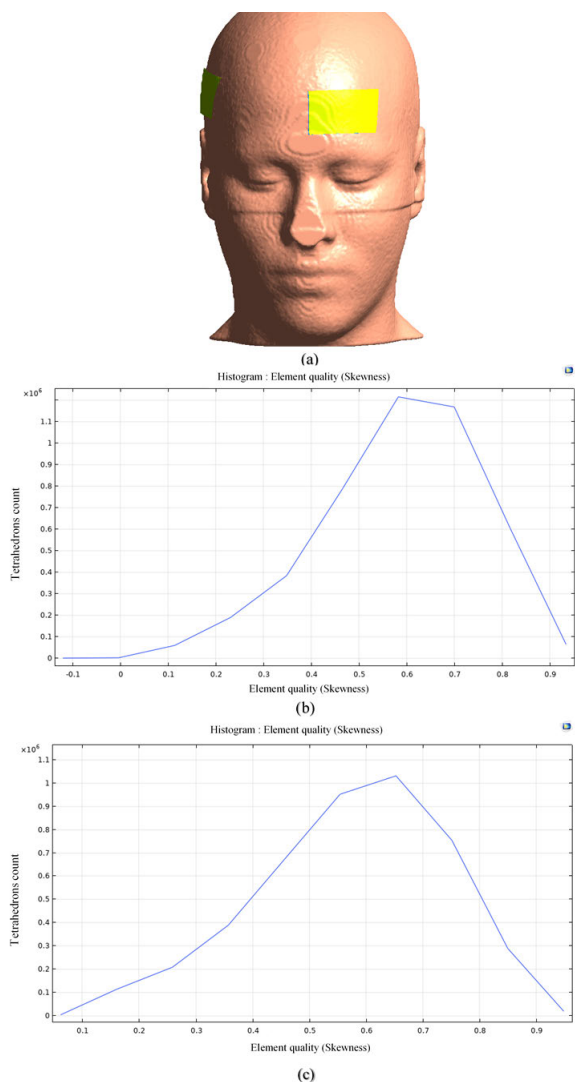
FIGURE 14. Example created from standard NY Head with corresponding skewness histogram (a) complete head model with electrodes positioned on it (b) show the skewness histogram before applying correcting algorithm in proposed toolbox where there is minus value this refer to the mesh contain degenerate tetrahedral (c) show the skewness after applying the correcting algorithm where all value at the accepted range between(0-1).

B. OPTIMIZATION IN POSITION AND SHAPE OF ELECTRODE

In this section, two experiments are performed using SimUTab which shows the effect of the position of the electrodes and their shapes on the concentration of electric field in the target area. The first one examines the effect of electrodes placement to increase the concentration of the electric field in a specific area of the brain. Simulation of the electric field using the proposed MATLAB toolbox can be employed to locate the electrodes correctly to increase the electric field density in the target region. In both experiments, the cathode electrode is mounted in the same location (in the right supraorbital region). In these expriments, the target area is below F3 according to the 10-20 international system which

is marked with a red circle as shown in Fig. 15. This location is roughly close to the lower part of the dorsolateral prefrontal cortex (DL_PFC). Fig. 15(a), shows the Electric field density distribution of the cerebral cortex when the anode electrode placed in FC3 position. The size of electrodes in the first experiment (for both anode and cathode) is considered to be 4 × 6 cm. As shown in Fig. 15, the distribution of electric field density is mainly constricted between two electrodes. Also, as shown in Fig. 15(b), when the position of the anode electrode changes to the F3 location (located between F3 and C3), electric field density increases in the target area.This experiment shows that the maximum electric density may not be concentrated directly under the active electrode, mainly when the distance between the electrodes is close.
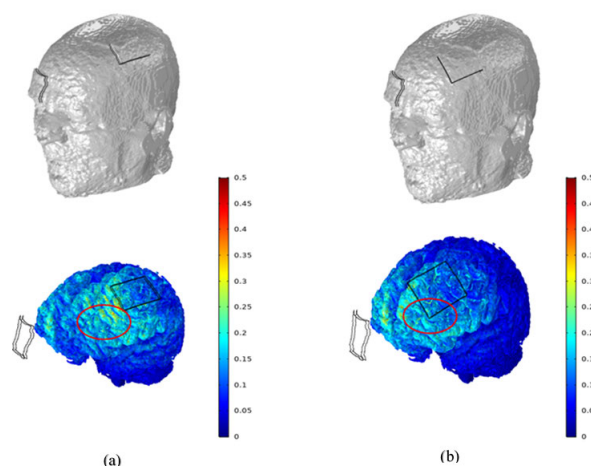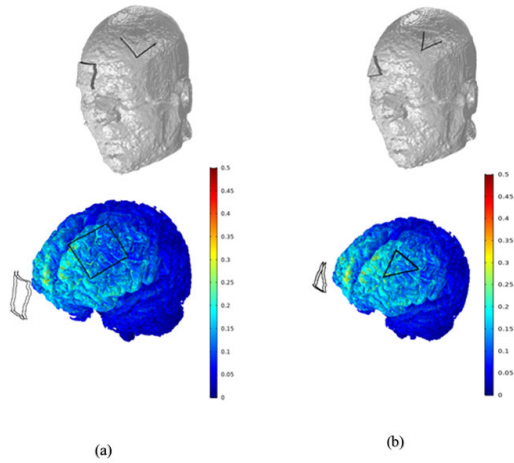

FIGURE 15. This experiment shows the effect of anode location on the electric field distribution in the target area. (a). anode at FC3 position increases the electric field density in the target area (marked with a red circle) while it is farther away from the target area. (b). anode at F3 position does not concentrate the electric field in the target area, although the anode position is close to it (both positions are compatible with 10-20 international system).

In the next experiment, the F3 location is again chosen as the target area and the electrode shape is changed easily from rectangle to triangle using the proposed toolbox. As shown in Fig. 16, this change leads to increase electric field density in the cerebral cortex. The above experiments demonstrate how SimUTab can be utilized to select the appropriate location and optimal shape for the electrodes, to increase the electric field density at the target location.

C. COMPARISONS WITH OTHER PIPELINES

We compare the performance of SimUTab with other famous toolboxes. For this purpose, Roast [21] and SimNib [29] have been selected, where they are considered as popular programs in this field. For comparison, at first a same head model from standard MRI data is selected and then its volume meshing (as well as electric field simulation) are performed using SimUTab and two other methods (mentioned above). Two criteria including the quality of output mesh and the simulation of the electric field distribution are considered to

FIGURE 16. This experiment shows how the changing electrode shape can effect the concentration of electric field in the target area. (a). distribution of electric field on the cerebral cortex, when the shape of electrodes is rectangle (b). distribution of electric field on the cerebral cortex, when the shape of electrodes is triangular.


FIGURE 17. Comparison the histogram of quality distributions for tetrahedral meshes (which generated by different toolboxes). (a) Histogram of Joe-Liu (η) (b) radius-edge ratio (α) (c) inscribed-circumscribed radius sphere ratio (ρ).

FIGURE 18. (a) Anatomical representation of GM produced by SimNib in the default settings (number of nodes=906810, number of triangles =1113028,number of tetrahedrons: 5012052) (b) anatomical representation of GM in SimNib toolbox when the node density is reduced(number of nodes=180546, number of triangles =298132, number of tetrahedrons: 1092441).

make this comparison. In order to make a fair comparison in this section, as mentioned, a standard head model is employed for all three toolboxes; also, the shape of electrodes and their position are considered the same in experiments related to all toolboxes (in addition, the applied amount of current and inserted amount of gel are considered constant). For evaluating the quality of output meshes, three quality metrics (which are mentioned previously) are employed. The histograms of quality distributions for the mentioned metrics are shown in Fig. 17. As the results in Fig. 17 shows, the proposed method has improved in all quality metrics compared to other methods.

Also, the averaged values of η, α, and ρ for the proposed toolbox and two other methods are summarized in Table 4. The number of tetrahedrons and nodes in SimUTab is less than other methods which, despite being superior in all three quality criteria, leads to less computation cost. Since, each toolbox employs its own approach to generate tetrahedral mesh, the number of nodes and tetrahedrons in each toolbox are different (in the default settings). In another experiment, the mesh density produced by SimNib is reduced to approximately equal to the number of meshes in SimUtab (according to Table 4). Fig. 18(a) Shows anatomical representation of GM produced by SimNib in the default settings (number of tetrahedrons: 5012052); Fig. 18(b) also shows it after reducing the number of tetrahedrons to the number of SimUTab. As can be seen, the output head model loses much of its anatomical detail. Therefore, it can be concluded that each toolbox has its own settings and trying to unify some parameters such as mesh density, does not provide a suitable framework for comparison. Another experiment is performed also on the standard New York head model. In this experiment, anode and cathode electrodes are placed at Fp1 and FC4 respectively according to 10-20 EEG international system (rectangular electrodes of width 4cm, height 3cm, and
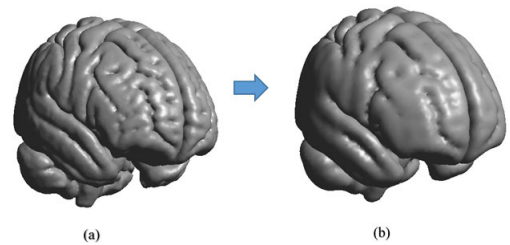
thickness 3mm). Simulating electric field distribution is performed by the proposed toolbox and other three methods in order to compare their performance. One of the most powerful tools for performing analysis and simulation is COMSOL, which is the most common finite element solver [55]–[57]. COMSOL accepts only high-quality meshes and is widely employed in neural simulation due to its accurate results. It is important to note that, due to accuracy issues the output mesh from other methods could not be imported to COMSOL without high refinement, which requires a high computational cost. While the high-quality mesh generated by the proposed toolbox satisfies the accuracy threshold requirement in COMSOL and any other finite element solver. However, the simulation is performed by four different methods (SimUTab, SimNib, Roast, and COMSOL). For accurate comparison, the location of the electrodes (also the amount of applied current) is considered the same in all experiments. Fig. 19 shows resulted electric field distribution on the cortical brain which are performed by the above methods. As the results show,

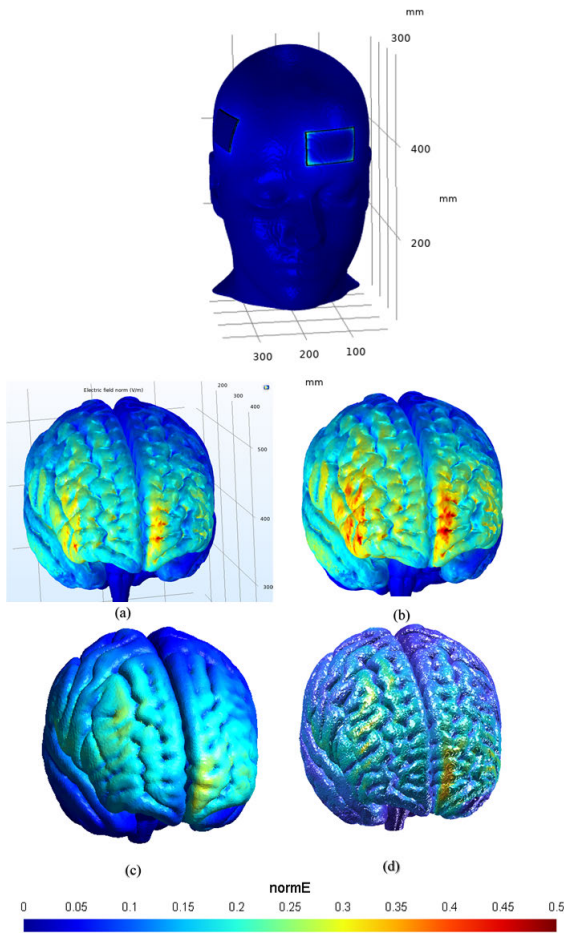there is no noticeable difference between SimUTab and other programs.

FIGURE 19. Electric field distribution on the cortical brain in gray matter using (a) COMSOL (b) proposed toolbox (SimUTab) (c) SimNib (d) Roast.

TABLE 4. Numerical results in order to compare produced meshes by different methods on the same head model. The number of tetrahedrons and nodes in the proposed toolbox is less than other methods which, despite being superior in all three quality criteria, leads to less computation cost.

Program	Tetra.-num.	Node num.	Value mean (ρ)	Value mean (α)	Value mean (η)
SimNib	5012052	906810	0.7102	0.5988	0.7441
Roast	2559491	447922	0.5497	0.4829	0.6166
Proposed toolbox(SimUTab)	904701	159592	0.6944	0.6416	0.7812

In the next experiment, the deviation of spatial distribution density between electric fields resulted from the proposed toolbox and the above methods are calculated. For this purpose, Spatial distribution of electric field is measured along the cutting line in the middle slice of the head using different methods as shown with a red arrow in Fig. 20(a). The measure

of the calculated electric field by the proposed toolbox is a little higher than the other methods as shown in Fig. 20(b). The small difference in magnitude can be explained by the increase in the number of high quality tetrahedral generated by the proposed toolbox. To quantify the deviation between the electric field distribution resulting by using SimUTab and other methods, equation 11 is employed.

$$div. = \frac{E_{tool} - E_x}{E_x} \times 100\% \qquad (11)$$

where E_{tool} represent the resulting electric field by the proposed toolbox and E_x represents the electric field generated by other methods. Fig. 18(b) shows the comparison between the electric field obtained by the proposed toolbox and other methods. As can be seen, there is not much difference in the spatial distribution of electric field; but the average of deviation (by averaging on equation 11) between the proposed method and SimNibs, Roast, and COMSOL is 15.1%, 23.4%, and 10.3%, respectively. As mentioned above, this difference is due to the improvement in the quality of generated tetrahedral mesh (by SimUTab), which despite the similarity in the spatial distribution of the electrical field, increases the spatial distribution density of the electric field.
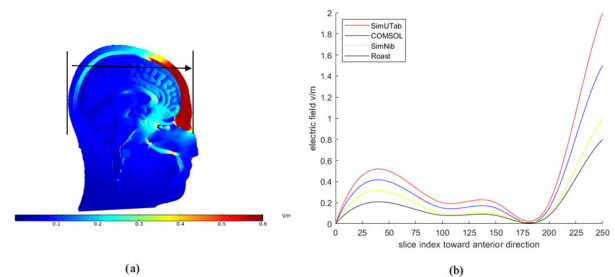

FIGURE 20. Calculating spatial distribution density of electric field using different methods i.e (SimUTab, SimNib, Roast, COMSOL) (a) show The middle slice of standared New York Head with electric field distribution (b) Comparison of the electric field distribution calculated along the black arrow between the proposed SimUTab and other methods.

V. CONCLUSION
In this paper, a new toolbox termed as SimUTab[a] for tDCS modeling is introduced. Our toolbox allows users to create state of the art models from individual MRIs without the need to have extensive experience to work with multiple complex software packages. The proposed method is implemented in a MATLAB environment in one place to leverage existing tools for image segmentation and 3D visualization. It employs different algorithms and open-source programs to create a high-quality mesh. A user-friendly GUI is implemented which permits even novice users to employ all functions of the toolbox and design custom electrode shapes and place them on the head (even in other than the standards forms). As demonstrated, SimUTab can be utilized to assess the

---

[a]The proposed toolbox (SimUTab) with several examples can be downloaded for free from GitHub: https://github.com/amjad1986/tDSC-TOOLBOX

investigation of optimal electrode position to increase the electric field density in a specific brain area. Generally, utilizing CGAL for surface mesh extraction in the proposed toolbox reduces computational time consumption and generates optimized mesh. specifically, the generated mesh is characterized by a low number of tetrahedral elements that have high- shape quality. Consequently, the proposed pipeline (As compared with previously published pipelines where MC is employed for surface extraction) is computationally efficient and has low memory consumption. For producing high-quality segmented tissues, a specific cleaning step is utilized to remove distortion. The surface generation is a long process in this work, where several algorithms are employed. Also, the surface mesh repairing process is applied with different free source fixing tools to generate high-quality triangular surfaces. After that, an open-source program TETGEN is employed to generate high-quality volume mesh. Projection of Electrodes surface mesh on skin surface mesh may produce some problems (such as intersection) that the proposed method manages them. Finally, experimental results evaluate and compare the presented toolbox with the other popular software packages. The results show the superiority and high ability of SimUTab toolbox. In the next version, a new algorithm for lesions segmentation based on artificial intelligence (AI) methods will be proposed.

REFERENCES

[1] B. Elsner, J. Kugler, and J. Mehrholz, "Transcranial direct current stimulation (tDCS) for improving aphasia after stroke: A systematic review with network meta-analysis of randomized controlled trials," *J. NeuroEng. Rehabil.*, vol. 17, no. 1, pp. 1–11, Dec. 2020.

[2] M. C. Gomez-Alvaro, S. Villafaina, J. L. Leon-Llamas, A. Murillo-Garcia, M. Melo-Alonso, J. Sánchez-Gómez, P. Molero, R. Cano-Plasencia, and N. Gusi, "Effects of transcranial direct current stimulation on brain electrical activity, heart rate variability, and dual-task performance in healthy and fibromyalgia women: A study protocol," *Behav. Sci.*, vol. 12, no. 2, p. 37, Feb. 2022.

[3] A. Mekonnen, S. Gholami-Boroujeny, I. Batkin, H. Caytak, and M. Bolic, "Temperature induced enhancement of tDCS efficacy," *Brain Stimulation*, vol. 10, no. 1, p. e1, Jan. 2017.

[4] S. Rush and D. A. Driscoll, "Current distribution in the brain from surface electrodes," *Anesthesia Analgesia*, vol. 47, no. 6, pp. 717–723, 1968.

[5] A. Datta, M. Elwassif, F. Battaglia, and M. Bikson, "Transcranial current stimulation focality using disc and ring electrode configurations: FEM analysis," *J. Neural Eng.*, vol. 5, no. 2, p. 163, 2008.

[6] P. Faria, M. Hallett, and P. C. Miranda, "A finite element analysis of the effect of electrode area and inter-electrode distance on the spatial distribution of the current density in tDCS," *J. Neural Eng.*, vol. 8, no. 6, Dec. 2011, Art. no. 066017.

[7] C. Poreisz, K. Boros, A. Antal, and W. Paulus, "Safety aspects of transcranial direct current stimulation concerning healthy subjects and patients," *Brain Res. Bull.*, vol. 72, nos. 4–6, pp. 208–214, May 2007.

[8] H.-I. Kuo, M. Bikson, A. Datta, P. Minhas, W. Paulus, M.-F. Kuo, and M. A. Nitsche, "Comparing cortical plasticity induced by conventional and high-definition 4 × 1 ring tDCS: A neurophysiological study," *Brain Stimulation*, vol. 6, no. 4, pp. 644–648, Jul. 2013.

[9] G. S. Shekhawat and S. Vanneste, "Optimization of transcranial direct current stimulation of dorsolateral prefrontal cortex for tinnitus: A nonlinear dose-response effect," *Sci. Rep.*, vol. 8, no. 1, pp. 1–8, Dec. 2018.

[10] L. Golestanirad, B. Elahi, A. Molina, J. R. Mosig, C. Pollo, R. Chen, and S. J. Graham, "Analysis of fractal electrodes for efficient neural stimulation," *Frontiers Neuroeng.*, vol. 6, pp. 1–3, Jul. 2013.

[11] S. Mahdavi, F. Towhidkhah, and N. Fatouraee, "Efficacy of fractal electrodes in transcranial direct current stimulation: A computational modeling study," in *Proc. 23rd Iranian Conf. Electr. Eng.*, May 2015, pp. 99–103.

[12] A. Amani, M. Yousefian, H. Seyedarabi, and M. Farhoudi, "Effect of triangular electrode schemes on Broca's cortical stimulation: Conventional and HD-tDCS study," *Med. Biol. Eng. Comput.*, vol. 59, no. 4, pp. 913–924, Apr. 2021.

[13] P. C. Miranda, M. Lomarev, and M. Hallett, "Modeling the current distribution during transcranial direct current stimulation," *Clin. Neurophysiol.*, vol. 117, no. 7, pp. 1623–1629, Jul. 2006.

[14] A. H. Javadi and V. Walsh, "Transcranial direct current stimulation (tDCS) of the left dorsolateral prefrontal cortex modulates declarative memory," *Brain Stimulation*, vol. 5, no. 3, pp. 231–241, Jul. 2012.

[15] R. Sparing, M. D. Hesse, and G. R. Fink, "Neuronavigation for transcranial magnetic stimulation (TMS): Where we are and where we are going," *Cortex*, vol. 46, no. 1, pp. 118–120, Jan. 2010.

[16] A. T. Sack, R. Cohen Kadosh, T. Schuhmann, M. Moerel, V. Walsh, and R. Goebel, "Optimizing functional accuracy of TMS in cognitive studies: A comparison of methods," *J. Cognit. Neurosci.*, vol. 21, no. 2, pp. 207–221, Feb. 2009.

[17] Y. Huang, J. P. Dmochowski, Y. Su, A. Datta, C. Rorden, and L. C. Parra, "Automated MRI segmentation for individualized modeling of current flow in the human head," *J. Neural Eng.*, vol. 10, no. 6, Dec. 2013, Art. no. 066004.

[18] G. D'Inzeo, K. P. Esselle, S. Pisa, and M. A. Stuchly, "Comparison of homogeneous and heterogeneous tissue models for coil optimization in neural stimulation," *Radio Sci.*, vol. 30, no. 1, pp. 245–253, Jan. 1995.

[19] P. Ciechanski, H. L. Carlson, S. S. Yu, and A. Kirton, "Modeling transcranial direct-current stimulation-induced electric fields in children and adults," *Frontiers Hum. Neurosci.*, vol. 12, p. 268, Jul. 2018.

[20] D. Truong, P. Minhas, A. Mokrejs, and M. Bikson, "A role of computational modeling in customization of transcranial direct current," in *Textbook of Neuromodulation: Principles, Methods and Clinical Applications*, 2014, p. 113.

[21] Y. Huang, A. Datta, M. Bikson, and L. C. Parra, "Realistic volumetricapproach to simulate transcranial electric stimulation—ROAST—A fully automated open-source pipeline," *J. neural Eng.*, vol. 16, no. 5, 2019, Art. no. 056006.

[22] R. Oostenveld, P. Fries, E. Maris, and J.-M. Schoffelen, "FieldTrip: Open source software for advanced analysis of MEG, EEG, and invasive electrophysiological data," *Comput. Intell. Neurosci.*, vol. 2011, pp. 1–9, Oct. 2011.

[23] Y.-J. Jung, J.-H. Kim, and C.-H. Im, "COMETS: A MATLAB toolbox for simulating local electric fields generated by transcranial direct current stimulation (tDCS)," *Biomed. Eng. Lett.*, vol. 3, no. 1, pp. 39–46, Mar. 2013.

[24] A. P. Tran and Q. Fang, "Fast and high-quality tetrahedral mesh generation from neuroanatomical scans," 2017, *arXiv:1708.08954*.

[25] J. Ashburner *et al.*, "SPM12 manual," Wellcome Trust Centre Neuroimag., London, U.K., Tech. Rep., vol. 2464, 2014.

[26] J. Shen. (2022). *Tools for NIfTI and ANALYZE Image*. [Online]. Available: https://www.mathworks.com/matlabcentral/fileexchange/-8797-tools-for-nifti-and-analyze-image

[27] Y. Huang, L. C. Parra, and S. Haufe, "The New York head—A precise standardized volume conductor model for EEG source localization and tES targeting," *NeuroImage*, vol. 140, pp. 150–162, Oct. 2016.

[28] J. Ashburner and K. J. Friston, "Unified segmentation," *NeuroImage*, vol. 26, no. 3, pp. 839–851, 2005.

[29] M. Windhoff, A. Opitz, and A. Thielscher, "Electric field calculations in brain stimulation based on finite elements: An optimized processing pipeline for the generation and usage of accurate individual head models," *Hum. Brain Mapping*, vol. 34, no. 4, pp. 923–935, Apr. 2013.

[30] J. D. Nielsen, K. H. Madsen, O. Puonti, H. R. Siebner, C. Bauer, C. G. Madsen, G. B. Saturnino, and A. Thielscher, "Automatic skull segmentation from MR images for realistic volume conductor models of the head: Assessment of the state-of-the-art," *NeuroImage*, vol. 174, pp. 587–598, Jul. 2018.

[31] J.-D. Boissonnat and S. Oudot, "Provably good sampling and meshing of surfaces," *Graph. Models*, vol. 67, no. 5, pp. 405–451, Sep. 2005.

[32] C. Jamin, P. Alliez, M. Yvinec, and J.-D. Boissonnat, "CGALmesh: A generic framework for Delaunay mesh generation," *ACM Trans. Math. Softw.*, vol. 41, no. 4, pp. 1–24, Oct. 2015.

[33] N. Salman, "From 3D point clouds to feature preserving meshes," Ph.D. dissertation, Dept. Comput. Sci., Univ. Nice Sophia Antipolis, 2010.

[34] M. Attene and B. Falcidieno, "ReMESH: An interactive environment to edit and repair triangle meshes," in *Proc. IEEE Int. Conf. Shape Modeling Appl.*, Jun. 2006, p. 41.

[35] M. Attene, "A lightweight approach to repairing digitized polygon meshes," *Vis. Comput.*, vol. 26, no. 11, pp. 1393–1406, 2010.

[36] G. Bernstein. (2013). *Cork Boolean Library*. [Online]. Available: https://github.com/gilbo/cork

[37] H. Si, "TetGen, a Delaunay-based quality tetrahedral mesh generator," *ACM Trans. Math. Softw.*, vol. 41, no. 2, pp. 1–36, Jan. 2015.

[38] P. Gloor, "Neuronal generators and the problem of localization in electroencephalography: Application of volume conductor theory to electroencephalography," *J. Clin. Neurophysiol.*, vol. 2, no. 4, pp. 327–354, 1985.

[39] H. Si and K. Gärtner, "3D boundary recovery by constrained Delaunay tetrahedralization," *Int. J. Numer. Methods Eng.*, vol. 85, no. 11, pp. 1341–1364, Mar. 2011.

[40] N. Wang, M. Li, R. Ma, and L. Zhang, "Accuracy analysis of gradient reconstruction on isotropic unstructured meshes and its effects on inviscid flow simulation," *Adv. Aerodyn.*, vol. 1, no. 1, pp. 1–31, Dec. 2019.

[41] C. Marot and J.-F. Remacle, "Quality tetrahedral mesh generation with HXT," 2020, *arXiv:2008.08508*.

[42] Y. Zhang, C. Bajaj, and B.-S. Sohn, "3D finite element meshing from imaging data," *Comput. Methods Appl. Mech. Eng.*, vol. 194, nos. 48–49, pp. 5083–5106, Nov. 2005.

[43] X. Chen, J. Liu, Y. Pang, J. Chen, L. Chi, and C. Gong, "Developing a new mesh quality evaluation method based on convolutional neural network," *Eng. Appl. Comput. Fluid Mech.*, vol. 14, no. 1, pp. 391–400, Jan. 2020.

[44] A. Liu and B. Joe, "Relationship between tetrahedron shape measures," *BIT*, vol. 34, no. 2, pp. 268–287, Jun. 1994.

[45] Q. Du and D. Wang, "The optimal centroidal Voronoi tessellations and the Gersho's conjecture in the three-dimensional space," *Comput. Math. Appl.*, vol. 49, nos. 9–10, pp. 1355–1373, May 2005.

[46] H. Edelsbrunner, *Geometry and Topology for Mesh Generation*. Cambridge, U.K.: Cambridge Univ. Press, 2001.

[47] H. McCann, G. Pisano, and L. Beltrachini, "Variation in reported human head tissue electrical conductivity values," *Brain Topogr.*, vol. 32, no. 5, pp. 825–858, Sep. 2019.

[48] J. D. Jackson, *Classical Electrodynamics*. Hoboken, NJ, USA: Wiley, 1999.

[49] P. Dular, C. Geuzaine, F. Henrotte, and W. Legros, "A general environment for the treatment of discrete problems and its application to the finite element method," *IEEE Trans. Magn.*, vol. 34, no. 5, pp. 3395–3398, Sep. 1998.

[50] M. Segal, K. Akeley, C. Frazier, J. Leech, and P. Brown, "The OpenGL® graphics system: A specification (version 2.0)," Silicon Graphics Inc., Milpitas, CA, USA, Tech. Rep., vol. 22, 2004.

[51] P. M. Knupp, "Algebraic mesh quality metrics for unstructured initial meshes," *Finite Elements Anal. Des.*, vol. 39, pp. 217–241, Jan. 2003.

[52] *Introduction to COMSOL Multiphysics*, COMSOL Multiphysics, Burlington, MA, USA, 1998. Accessed: Feb. 9, 2018.

[53] G. Csifcsák, N. M. Boayue, O. Puonti, A. Thielscher, and M. Mittner, "Effects of transcranial direct current stimulation for treating depression: A modeling study," *J. Affect. Disorders*, vol. 234, pp. 164–173, Jul. 2018.

[54] A. Indahlastari, M. Chauhan, and R. J. Sadleir, "Benchmarking transcranial electrical stimulation finite element models: A comparison study," *J. Neural Eng.*, vol. 16, no. 2, Apr. 2019, Art. no. 026019.

[55] A. Datta, M. Elwassif, and M. Bikson, "Electrical stimulation of brain using a realistic 3D human head model: Improvement of spatial focality," in *Proc. Excerpt COMSOL Conf.*, 2008, pp. 1–5.

[56] N. Khadka, X. Liu, H. Zander, J. Swami, E. Rogers, S. F. Lempka, and M. Bikson, "Realistic anatomically detailed open-source spinal cord stimulation (RADO-SCS) model," *J. Neural Eng.*, vol. 17, no. 2, Apr. 2020, Art. no. 026033.

[57] L. Morales-Quezada, M. M. El-Hagrassy, B. Costa, R. A. McKinley, P. Lv, and F. Fregni, "Transcranial direct current stimulation optimization—From physics-based computer simulations to high-fidelity head phantom fabrication and measurements," *Frontiers Hum. Neurosci.*, vol. 13, p. 388, Oct. 2019.

AMJED Y. SAHIB was born in Al-Zubiadia, Wasit, Iraq, in 1986. He received the B.S. and M.S. degrees from the Electrical Engineering/Electronic and Communication Department, University of Baghdad, Iraq, in 2008 and 2013, respectively. He is currently pursuing the Ph.D. degree with the Communication Department, College of Electrical and Computer Engineering, University of Tabriz, Iran.

From 2013 to 2018, he worked as a Lecturer at the College of Engineering, University of Wasit. His research interests include quantum computer systems, image processing, artificial intelligent systems (AI), finite element method (FEM), and its application in electromagnetic systems. He has published some articles in this area.

HADI SEYEDARABI received the B.S. degree from the University of Tabriz, Tabriz, Iran, in 1993, the M.S. degree from the K. N. T. University of Technology, Tehran, Iran, in 1996, and the Ph.D. degree from the University of Tabriz, in 2006, all in electrical engineering. He is currently a Professor with the Faculty of Electrical and Computer Engineering, University of Tabriz. His research interests include image processing, computer vision, video coding, human–computer interaction, computational brain modeling and stimulation, deep learning applications in image processing, medical signal processing, and computer vision.

REZA AFROUZIAN received the Ph.D. degree in electrical engineering from the University of Tabriz, Tabriz, Iran, in 2015. He is currently an Assistant Professor with the Miyaneh Faculty of Engineering, University of Tabriz. His research interests include image processing, computer vision, pattern recognition, and machine learning.

MEHDI FARHOUDI received the General Medicine degree from the Tabriz University of Medical Science (TUOMS), Tabriz, Iran, in 1994. He is currently a Professor of neurology with the Imam REZA Medical Center, Neurology Department, Faculty of Medicine, and the Head of the Neurosciences Department, Advanced Faculty of Medicine, TUOMS. He is also the Head of the Stroke Team, Neurosciences Research Center (NSRC), Neurology Department, TUOMS. His research interests include cerebrovascular disease and Doppler studies. He is a member of the Iranian Neurology Association, the East Azerbaijan Multiple Sclerosis Society, and the World Stroke Organization. He was Certified by the Board in Neurology at the Imam Medical Center, TUOMS, in 1998.

• • •